Field-portable reflection and transmission microscopy based on lensless holography

Myungjun Lee,[1] Oguzhan Yaglidere,[1] and Aydogan Ozcan[1,2,3*]

[1]*Electrical Engineering Department, University of California at Los Angeles, CA 90095, USA*
[2]*Bioengineering Department, University of California at Los Angeles, CA 90095, USA*
[3]*California NanoSystems Institute (CNSI), University of California at Los Angeles, CA 90095, USA*
**ozcan@ucla.edu*

Abstract: We demonstrate a lensfree dual-mode holographic microscope that can image specimens in both transmission and reflection geometries using in-line transmission and off-axis reflection holography, respectively. This field-portable dual-mode holographic microscope has a weight of ~200 g with dimensions of 15 x 5.5 x 5cm, where a laser source is powered by two batteries. Based on digital in-line holography, our transmission microscope achieves a sub-pixel lateral resolution of ≤2 μm over a wide field-of-view (FOV) of ~24 mm^2 due to its unit fringe magnification geometry. Despite its simplicity and ease of operation, in-line transmission geometry is not suitable to image dense or connected objects such as tissue slides since the reference beam gets distorted causing severe aberrations in reconstruction of such objects. To mitigate this challenge, on the same cost-effective and field-portable assembly we built a lensless reflection mode microscope based on digital off-axis holography where a beam-splitter is used to interfere a tilted reference wave with the reflected light from the object surface, creating an off-axis hologram of the specimens on a CMOS sensor-chip. As a result of the reduced space-bandwidth product of the off-axis geometry compared to its in-line counterpart, the imaging FOV of our reflection mode is reduced to ~9 mm^2, while still achieving a similar sub-pixel resolution of ≤2 μm. We tested the performance of this compact dual-mode microscopy unit by imaging a US-air force resolution test target, various micro-particles as well as a histopathology slide corresponding to skin tissue. Due to its compact, cost-effective, and lightweight design, this dual-mode lensless holographic microscope might especially be useful for field-use or for conducting microscopic analysis in resource-poor settings.

OCIS codes: (090.1995) Digital holography; (180.0180) Microscopy; (170.1650) Coherence imaging

References and links

1. D. Gabor, "A new microscopic principle," Nature **161**(4098), 777–778 (1948).
2. J. W. Goodman, *Introduction to Fourier Optics* (Robert & Company, 2005), chaps. 3,4, and 9.
3. G. Liu and P. D. Scott, "Phase retrieval and twin-image elimination for in-line Fresnel holograms," J. Opt. Soc. Am. A **4**(1), 159–165 (1987).
4. U. Schnars and W. Jüptner, "Direct recording of holograms by a CCD target and numerical reconstruction," Appl. Opt. **33**(2), 179–181 (1994).
5. F. Dubois, L. Joannes, and J. C. Legros, "Improved three-dimensional imaging with a digital holography microscope with a source of partial spatial coherence," Appl. Opt. **38**(34), 7085–7094 (1999).
6. E. Cuche, P. Marquet, and C. Depeursinge, "Spatial filtering for zero-order and twin-image elimination in digital off-axis holography," Appl. Opt. **39**(23), 4070–4075 (2000).
7. W. Xu, M. H. Jericho, I. A. Meinertzhagen, and H. J. Kreuzer, "Digital in-line holography for biological applications," Proc. Natl. Acad. Sci. U.S.A. **98**(20), 11301–11305 (2001).
8. G. Pedrini and H. J. Tiziani, "Short-coherence digital microscopy by use of a lensless holographic imaging system," Appl. Opt. **41**(22), 4489–4496 (2002).
9. L. Repetto, E. Piano, and C. Pontiggia, "Lensless digital holographic microscope with light-emitting diode illumination," Opt. Lett. **29**(10), 1132–1134 (2004).

#150686 - $15.00 USD Received 7 Jul 2011; revised 11 Aug 2011; accepted 11 Aug 2011; published 30 Aug 2011

10. T.-C. Poon, "Recent progress in optical scanning holography," J. Hologr. Speckle **1**(1), 6–25 (2004).
11. B. Javidi, I. Moon, S. K. Yeom, and E. Carapezza, "Three-dimensional imaging and recognition of microorganism using single-exposure on-line (SEOL) digital holography," Opt. Express **13**(12), 4492–4506 (2005).
12. C. J. Mann, L. F. Yu, C. M. Lo, and M. K. Kim, "High-resolution quantitative phase-contrast microscopy by digital holography," Opt. Express **13**(22), 8693–8698 (2005).
13. J. Rosen, G. Indebetouw, and G. Brooker, "Homodyne scanning holography," Opt. Express **14**(10), 4280–4285 (2006).
14. J. Garcia-Sucerquia, W. Xu, S. K. Jericho, P. Klages, M. H. Jericho, and H. J. Kreuzer, "Digital in-line holographic microscopy," Appl. Opt. **45**(5), 836–850 (2006).
15. G. Popescu, T. Ikeda, R. R. Dasari, and M. S. Feld, "Diffraction phase microscopy for quantifying cell structure and dynamics," Opt. Lett. **31**(6), 775–777 (2006).
16. T. Colomb, F. Montfort, J. Kühn, N. Aspert, E. Cuche, A. Marian, F. Charrière, S. Bourquin, P. Marquet, and C. Depeursinge, "Numerical parametric lens for shifting, magnification, and complete aberration compensation in digital holographic microscopy," J. Opt. Soc. Am. A **23**(12), 3177–3190 (2006).
17. F. Dubois, C. Yourassowsky, O. Monnom, J.-C. Legros, O. Debeir, P. Van Ham, R. Kiss, and C. Decaestecker, "Digital holographic microscopy for the three-dimensional dynamic analysis of in vitro cancer cell migration," J. Biomed. Opt. **11**(5), 054032 (2006).
18. G. Situ and J. T. Sheridan, "Holography: an interpretation from the phase-space point of view," Opt. Lett. **32**(24), 3492–3494 (2007).
19. A. Stern and B. Javidi, "Theoretical analysis of three-dimensional imaging and recognition of micro-organisms with a single-exposure on-line holographic microscope," J. Opt. Soc. Am. A **24**(1), 163–168 (2007).
20. S. S. Kou and C. J. Sheppard, "Imaging in digital holographic microscopy," Opt. Express **15**(21), 13640–13648 (2007).
21. J. Rosen and G. Brooker, "Non-scanning motionless fluorescence three-dimensional holographic microscopy," Nat. Photonics **2**(3), 190–195 (2008).
22. U. Gopinathan, G. Pedrini, and W. Osten, "Coherence effects in digital in-line holographic microscopy," J. Opt. Soc. Am. A **25**(10), 2459–2466 (2008).
23. V. Micó, Z. Zalevsky, C. Ferreira, and J. García, "Superresolution digital holographic microscopy for three-dimensional samples," Opt. Express **16**(23), 19260–19270 (2008).
24. J. Di, J. Zhao, H. Jiang, P. Zhang, Q. Fan, and W. Sun, "High resolution digital holographic microscopy with a wide field of view based on a synthetic aperture technique and use of linear CCD scanning," Appl. Opt. **47**(30), 5654–5659 (2008).
25. N. T. Shaked and J. Rosen, "Multiple-viewpoint projection holograms synthesized by spatially incoherent correlation with broadband functions," J. Opt. Soc. Am. A **25**(8), 2129–2138 (2008).
26. M. M. Hossain, D. S. Mehta, and C. Shakher, "Information reduction using lensless Fourier transform digital composite holography," Opt. Laser Technol. **40**(1), 120–128 (2008).
27. D. J. Brady, K. Choi, D. L. Marks, R. Horisaki, and S. Lim, "Compressive holography," Opt. Express **17**(15), 13040–13049 (2009).
28. T. R. Hillman, T. Gutzler, S. A. Alexandrov, and D. D. Sampson, "High-resolution, wide-field object reconstruction with synthetic aperture Fourier holographic optical microscopy," Opt. Express **17**(10), 7873–7892 (2009).
29. L. Waller, Y. Luo, S. Y. Yang, and G. Barbastathis, "Transport of intensity phase imaging in a volume holographic microscope," Opt. Lett. **35**(17), 2961–2963 (2010).
30. N. T. Shaked, T. M. Newpher, M. D. Ehlers, and A. Wax, "Parallel on-axis holographic phase microscopy of biological cells and unicellular microorganism dynamics," Appl. Opt. **49**(15), 2872–2878 (2010).
31. M. K. Kim, "Principles and techniques of digital holographic microscopy," SPIE Rev. **1**(1), 018005 (2010).
32. O. Mudanyali, D. Tseng, C. Oh, S. O. Isikman, I. Sencan, W. Bishara, C. Oztoprak, S. Seo, B. Khademhosseini, and A. Ozcan, "Compact, light-weight and cost-effective microscope based on lensless incoherent holography for telemedicine applications," Lab Chip **10**(11), 1417–1428 (2010).
33. D. Tseng, O. Mudanyali, C. Oztoprak, S. O. Isikman, I. Sencan, O. Yaglidere, and A. Ozcan, "Lensfree microscopy on a cellphone," Lab Chip **10**(14), 1787–1792 (2010).
34. L. Miccio, A. Finizio, R. Puglisi, D. Balduzzi, A. Galli, and P. Ferraro, "Dynamic DIC by digital holography microscopy for enhancing phase-contrast visualization," Biomed. Opt. Express **2**(2), 331–344 (2011).
35. J. Hahn, S. Lim, K. Choi, R. Horisaki, and D. J. Brady, "Video-rate compressive holographic microscopic tomography," Opt. Express **19**(8), 7289–7298 (2011).
36. W. Bishara, U. Sikora, O. Mudanyali, T.-W. Su, O. Yaglidere, S. Luckhart, and A. Ozcan, "Holographic pixel super-resolution in portable lensless on-chip microscopy using a fiber-optic array," Lab Chip **11**(7), 1276–1279 (2011).
37. S. O. Isikman, W. Bishara, S. Mavandadi, F. W. Yu, S. Feng, R. Lau, and A. Ozcan, "Lens-free optical tomographic microscope with a large imaging volume on a chip," Proc. Natl. Acad. Sci. U.S.A. **108**(18), 7296–7301 (2011), doi:10.1073/pnas.1015638108.
38. S. O. Isikman, W. Bishara, U. Sikora, O. Yaglidere, J. Yeah, and A. Ozcan, "Field-portable lensfree tomographic microscope," Lab Chip **11**(13), 2222–2230 (2011).
39. D. N. Breslauer, R. N. Maamari, N. A. Switz, W. A. Lam, and D. A. Fletcher, "Mobile phone based clinical microscopy for global health applications," PLoS ONE **4**(7), e6320 (2009).
40. L. M. Lee, X. Cui, and C. Yang, "The application of on-chip optofluidic microscopy for imaging *Giardia lamblia* trophozoites and cysts," Biomed. Microdevices **11**(5), 951–958 (2009).

#150686 - $15.00 USD Received 7 Jul 2011; revised 11 Aug 2011; accepted 11 Aug 2011; published 30 Aug 2011

41. A. R. Miller, G. L. Davis, Z. M. Oden, M. R. Razavi, A. Fateh, M. Ghazanfari, F. Abdolrahimi, S. Poorazar, F. Sakhaie, R. J. Olsen, A. R. Bahrmand, M. C. Pierce, E. A. Graviss, and R. Richards-Kortum, "Portable, battery-operated, low-cost, bright field and fluorescence microscope," PLoS ONE **5**(8), e11890 (2010).
42. H. Zhu, O. Yaglidere, T. W. Su, D. Tseng, and A. Ozcan, "Cost-effective and compact wide-field fluorescent imaging on a cell-phone," Lab Chip **11**(2), 315–322 (2011).
43. Z. J. Smith, K. Chu, A. R. Espenson, M. Rahimzadeh, A. Gryshuk, M. Molinaro, D. M. Dwyre, S. Lane, D. Matthews, and S. Wachsmann-Hogiu, "Cell-phone-based platform for biomedical device development and education applications," PLoS ONE **6**(3), e17150 (2011).
44. A. F. Coskun, I. Sencan, T. W. Su, and A. Ozcan, "Wide-field lensless fluorescent microscopy using a tapered fiber-optic faceplate on a chip," Analyst (Lond.) **136**(17), 3512–3518 (2011).
45. W. P. Mutter and R. S. Brown, "Point-of-care photomicroscopy of urine," N. Engl. J. Med. **364**(19), 1880–1881 (2011).
46. J. D. Bancroft and M. Gamble, *Theory and Practice of Histological Techniques* (Elsevier Health Sciences, 2007).

1. Introduction

Since its invention by Gabor [1] holography has experienced massive growth as a field [2–38], which got even faster as various technologies such as digital sensor-arrays (e.g., CMOS and CCD technologies) and personal computers became more powerful and cost-effective, making them ubiquitous. In specific, digital holographic microscopy (DHM) has recently attracted significant attention for its ability to retrieve both amplitude and phase information of specimens for various applications in physical and biomedical sciences [4–38]. These recent advances in DHM techniques also create unique opportunities to simplify the architecture of conventional bench-top microscopes, while also providing a decent imaging performance over large sample volumes, which is an important need in general for e.g., high-throughput imaging/screening applications. Note also that, apart from holographic techniques, there have been several other efforts [39–45] toward the same goal, aiming to create much simpler microscopes that can even work in resource-limited environments.

Along the same lines, here we demonstrate a field-portable lensfree holographic microscope that can image specimens both in reflection and transmission modes within a lightweight (~200 g) and cost-effective platform. This lensfree dual-mode microscope, in its reflection mode of operation, is based on off-axis holography, where the reflected light from a specimen interferes with a separate reference beam at a digital sensor-array. This off-axis reflection hologram is then processed in the Fourier domain to filter out the undesired terms such that an image of the specimen can be digitally reconstructed using a PC. In its transmission mode of operation, however, the same microscopy platform is based on digital in-line holography to reconstruct transmission images of objects that are placed rather close to the sensor-chip. In our design, each mode of operation has its own advantages and disadvantages. For instance, the reflection geometry is especially suitable for imaging of optically dense or spatially connected specimen (such as tissue slides) where in-line transmission geometry would fail due to spatial distortions of the reference wave. On the other hand, the transmission geometry of this dual-mode lensfree microscope is easier to align and operate, and in addition, it achieves a much larger imaging field-of-view (FOV) compared to its off-axis reflection counterpart.

We experimentally demonstrated the performance of this field-portable dual-mode microscopy unit by imaging US-air force resolution test targets (confirming a spatial resolution of ≤ 2 μm for both the reflection and transmission modes), various micro-particles and a histopathology slide corresponding to skin tissue. Since it provides a compact, cost-effective, and lightweight microscopy interface, this lensfree holographic microscope might find use in resource-limited settings and field applications involving e.g., global health challenges.

2. System design

2.1. Reflection mode off-axis lensfree holographic microscopy

Our reflection mode lensfree microscope is based on *off-axis* digital holography. Figure 1 shows a schematic diagram and a photograph of our lensfree reflection mode microscope utilizing a Michelson interferometer geometry. In this architecture, a 20-mW green laser diode

#150686 - $15.00 USD Received 7 Jul 2011; revised 11 Aug 2011; accepted 11 Aug 2011; published 30 Aug 2011

(λ = 531 nm - powered by two AA batteries) is butt-coupled to a 3-μm pin-hole (PH) *without* the use of any light-coupling optics. We chose to work with a relatively large aperture in our design to keep it simple and compact by avoiding any light-coupling components such as a micro-mechanical alignment stage or an objective lens. The laser light passing through the PH then illuminates a 10-mm beam cube (BC) to split into two beams, as shown in Fig. 1(a). The first beam is directed toward the specimen and is then reflected back, while the other is directed to a reference mirror that is slightly tilted (with an angle of θ, e.g., ~5°). These two reflected waves interfere at a 5-Mpixel CMOS sensor-chip (Model: MT9P031, Micron Technology) which has a pixel size of 2.2 μm and an active area of ~24 mm^2, creating a lensfree off-axis reflection hologram of the sample. Note that by using a smaller pixel size sensor-chip (e.g., ≤1.4 μm) a larger tilt angle can also be utilized in our hologram recording geometry. Typical exposure times in our lensfree images were ≤200 ms. Figures 1(b)-(c) show schematics of this compact reflection-mode lensless DHM weighting only ~200 g which includes its case and two AA batteries.

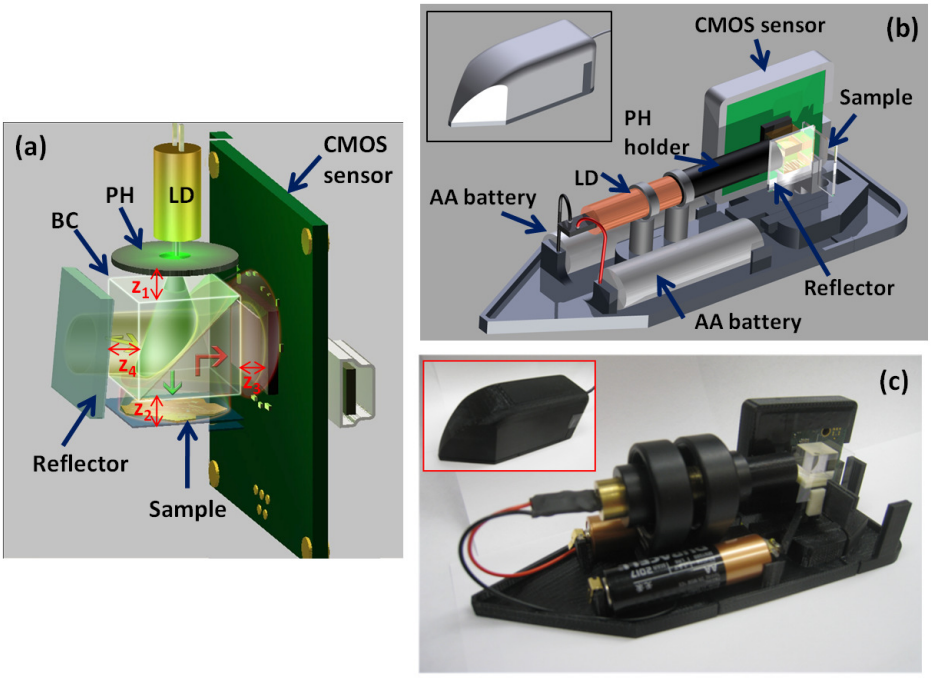

Fig. 1. (a-c) Schematic diagram and photograph of our lensfree off-axis reflection holographic microscope are shown (LD: laser diode, PH: pin-hole, BC: beam-cube). The LD and the CMOS sensor chip are powered by two AA batteries and a USB connection, respectively. The inset image in (c) shows the field-portable microscope with its cover. This entire assembly, including the batteries, weighs ~200 g with dimensions of 15 x 5.5 x 5 cm.

In this lensfree reflection imaging geometry, the diameter of the PH, the pixel size at the sensor, and the wavelength of illumination are important factors that determine the achievable spatial resolution. Unlike partially coherent lensfree holographic digital in-line microscopy [32,33], the effect of the pinhole size on spatial coherence diameter at the sensor plane is not critical here since we already employ coherent laser illumination. Instead, the illumination numerical aperture (NA) is determined by the emission cone angle of the light passing through the PH, and a diameter of 3 μm in our set-up provided an illumination NA of ~0.17 at λ = 531 nm [7,14]. For an optimum imaging system design, this illumination NA should be adjusted such that it uniformly covers the specimen FOV as well as the sensor-array active area. For a PH diameter of 3 μm, we designed our system such that we had a PH-to-sample distance (z_{PS}) of ~16.5 mm and a sample-to-sensor distance (z_{SS}) of ~11 mm, where z_1 ≈5.5

#150686 - $15.00 USD Received 7 Jul 2011; revised 11 Aug 2011; accepted 11 Aug 2011; published 30 Aug 2011

mm, $z_2 \leq 1$ mm, and $z_3 \leq 1$ mm, as shown in Fig. 1(a). This hologram recording geometry provides a fringe magnification of $F = (z_{PS} + z_{SS}) / z_{PS} \sim 1.67$ for the reflected object beam, resulting in an imaging FOV of ~3.4 x 2.6 mm at the object plane [7]. This ensures that the illumination cone angle provides sufficiently wide spatial coverage for both the sample area (~3.4 x 2.6 mm) and the sensor active area (5.70 x 4.28 mm).

Apart from the illumination cone, the detection numerical aperture (determined by the sensor width and z_{SS}) is another important factor that would affect the spatial resolution in our scheme. By limiting the sample-to-sensor distance to almost the beam-cube width (i.e., z_{SS} ~11 mm - see Fig. 1(a)), using a CMOS sensor with an active area of ~5.70 x 4.28 mm, we can achieve a detection NA of ~0.2, which provides a close match to the illumination NA provided by the PH.

In addition to these, since the specimen is placed rather close to the sensor-chip, the pixel size at the CMOS chip would be another limiting factor for our resolution, potentially causing spatial aliasing. Because of our relatively small fringe magnification factor (F ~1.67), the pixel size at the sensor (i.e., 2.2 μm) effectively scales down to ~1.3 μm, which could be considered as an important source of resolution limit in our geometry. Note that in our off-axis scheme since θ is relatively small (~5°), this pixel size is still sufficient to sample the interference between the reference and the reflection beams in our set-up [6].

One final source of resolution limitation that we would like to discuss here is due to the spatial averaging effect of the pinhole illumination. Since we use a relatively large PH diameter of 3 μm (to keep the design simple and compact by avoiding any light-coupling components), this aperture function is convolved with the spatial features of the specimen. However, this convolution operation is effectively scaled down by $z_{PS} / z_{SS} \approx 1.5$ such that an effective PH diameter of ~2 μm is introduced at the hologram/sensor plane [32]. Since our physical pixel size at the sensor chip is already 2.2 μm, this can be considered as a secondary limitation compared to pixelation (i.e., spatial aliasing) that is discussed in the previous paragraph.

For digital reconstruction of our off-axis holograms, the raw reflection interference data first need to be digitally filtered in the Fourier domain to remove the zero-order term, twin image artifact and multiple-reflection noise terms, while keeping the spatial frequency components of the real image [6,16]. We then use the Fresnel approximation [6,31,35] to the Fresnel-Kirchhoff integral [2] to digitally create the object image from this filtered Fourier data. Since we work with a relatively low numerical aperture of e.g., ≤0.2, the Fresnel approximation is still valid here, which provides a decent reconstruction result (achieving ≤2 μm resolution in reflection) without suffering from a computational bottleneck [35]. In this work, all our reconstructions were implemented in Matlab using a PC (Intel(R) Core(TM)2 Duo CPU E7500 - 2.93GHz), and typical reconstruction times were less 120 s (for the entire FOV), which could be significantly improved using e.g., a graphics processing unit.

2.2. Transmission mode in-line lensfree holographic microscopy

In its transmission mode, the same microscopy platform changes the position of the CMOS sensor chip and removes the beam-splitter cube (see Fig. 2), such that lensfree diffraction holograms of the specimens can be recorded on the sensor-array. In this transmission geometry shown in Fig. 2, the scattered light from each individual cell or particle interferes with the un-scattered light (which acts as the reference beam) generating an in-line hologram on the CMOS sensor plane [7].

The basic design of this lensfree transmission microscopy platform is similar to our previous work [32,33] such that it employs a unit fringe magnification geometry with a sample-to-sensor distance of < 1 mm and a pinhole-to-sample distance of ~25 mm. In this geometry, the illumination cone generated by our PH is still sufficient to practically create uniform illumination across the sample and the sensor planes. In addition to this, the relatively large PH size (~3 μm) does *not* pose any limitations to achievable spatial resolution (unlike the reflection mode discussed earlier) since there is a large demagnification factor of > 25 fold

#150686 - $15.00 USD Received 7 Jul 2011; revised 11 Aug 2011; accepted 11 Aug 2011; published 30 Aug 2011

in this hologram recording geometry (i.e., $z_{PS} > 25\ z_{SS}$). Another important advantage of this hologram recording scheme is its large imaging FOV, which is the same as the active area of the sensor chip since $F \sim 1$, i.e., FOV = 24 mm^2 in our lensless microscope shown in Fig. 2.

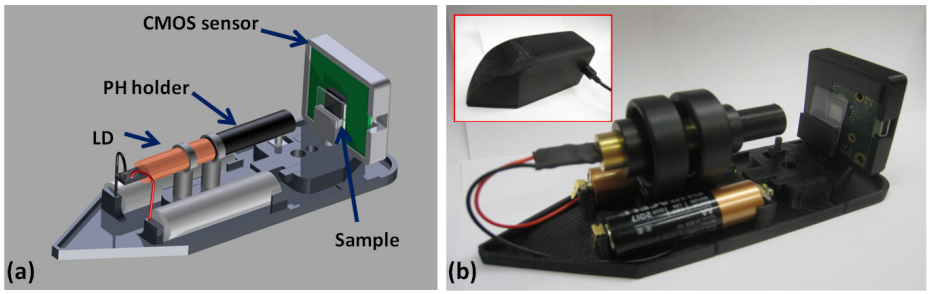

Fig. 2. (a) Schematic diagram and (b) photograph of our lensless in-line transmission mode holographic microscope are shown. The inset image in (b) shows the field-portable microscope with its cover. The PH-to-sample distance is ~25 mm and the sample-to-sensor distance is ≤1 mm, such that the entire 24 mm^2 active area of the CMOS sensor becomes the sample FOV.

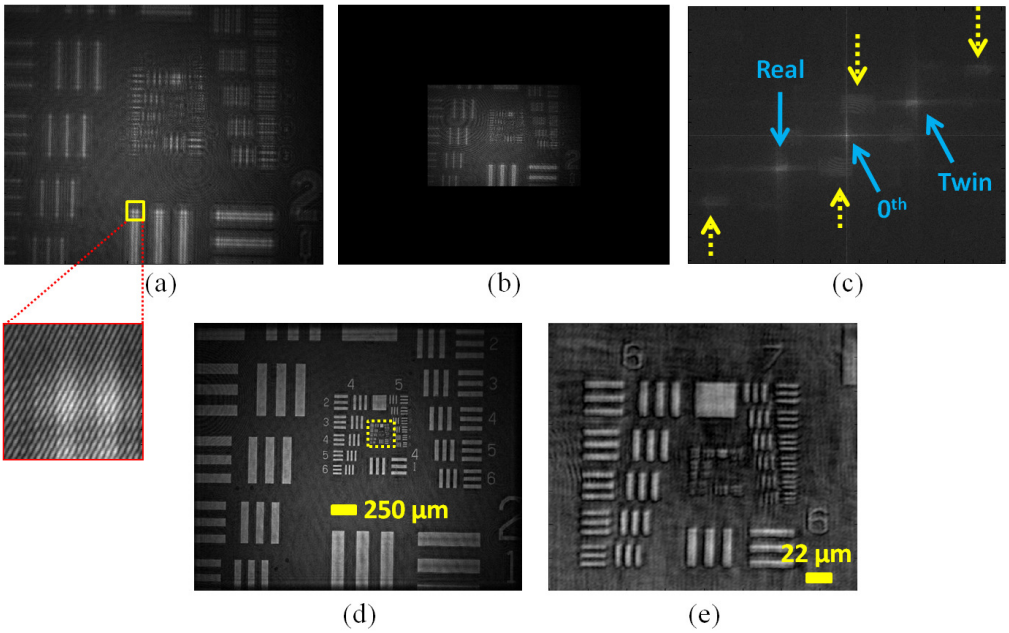

Fig. 3. Reconstruction procedures for off-axis geometry using the lensfree reflection DHM shown in Fig. 1 are described. (a) The raw off-axis lensfree reflection hologram of US-AFT. The interference fringes of off-axis geometry are shown in the expanded version of the yellow rectangular box. (b) Pixel interpolated and zero-padded reflection hologram. (c) Fourier spectrum of this reflection hologram, which includes spatial frequencies of the 0th order, real and twin images, as well as parasitic-reflections which are indicated by dashed arrows. (d) The reconstructed reflection hologram image over a large FOV of ~9 mm^2. (e) The digitally zoomed region specified with the small yellow rectangle in Fig. 3(d) is shown here, which demonstrates a spatial resolution of ≤2µm.

On the other hand, similar to the reflection mode off-axis scheme described earlier, the finite pixel size at the sensor chip is still a limitation for spatial resolution due to under-sampling of in-line transmission holograms. As discussed in our earlier work [36–38], this limitation, however, can be mitigated in various ways to achieve a sub-pixel spatial resolution of ≤2 µm using a pixel size of e.g., 2.2 µm as employed in our experiments. Before we discuss these experimental results, we would like to emphasize that, despite its architectural and

#150686 - $15.00 USD Received 7 Jul 2011; revised 11 Aug 2011; accepted 11 Aug 2011; published 30 Aug 2011

alignment simplicity, in-line transmission geometry of Fig. 2 would not be suitable for imaging of connected or optically thick objects (such as tissue slides) where the in-line reference beam picks up spatial distortion. Therefore for such connected or thick specimens the off-axis reflection mode of our lensfree microscopy platform would be a better choice.

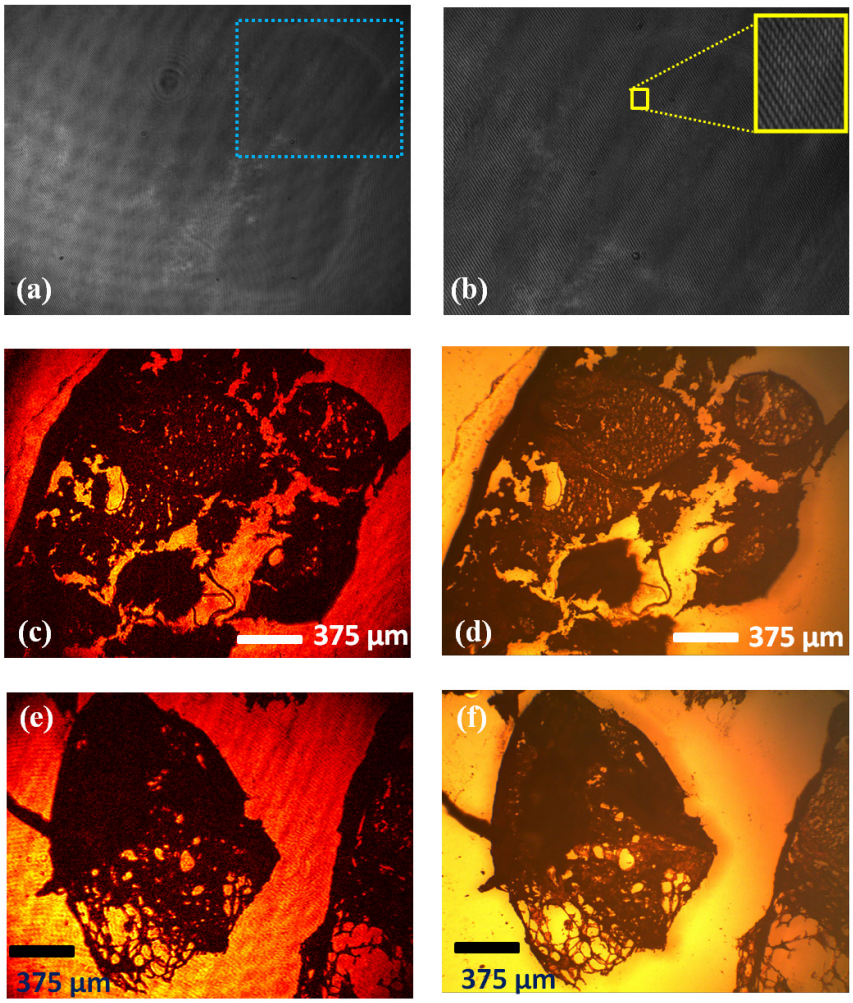

Fig. 4. Reflection imaging of a histopathology slide corresponding to skin tissue using lensfree off-axis holography. (a) The raw off-axis reflection hologram of skin tissue. (b) The digitally zoomed hologram region specified with the blue rectangle in Fig. 4(a) is shown. The corresponding reconstructed amplitude reflection image is shown in (c). Conventional reflection mode microscope image of the same specimen using a 4X objective lens (NA: 0.1) is also shown in (d) for comparison purposes. Note that due to their limited FOV, higher magnification objective lenses would not be able to capture the same comparison image. (e) same as in (c) except for a different region of interest. (f) provides a conventional reflection mode microscope image of the same specimen for comparison.

#150686 - $15.00 USD Received 7 Jul 2011; revised 11 Aug 2011; accepted 11 Aug 2011; published 30 Aug 2011

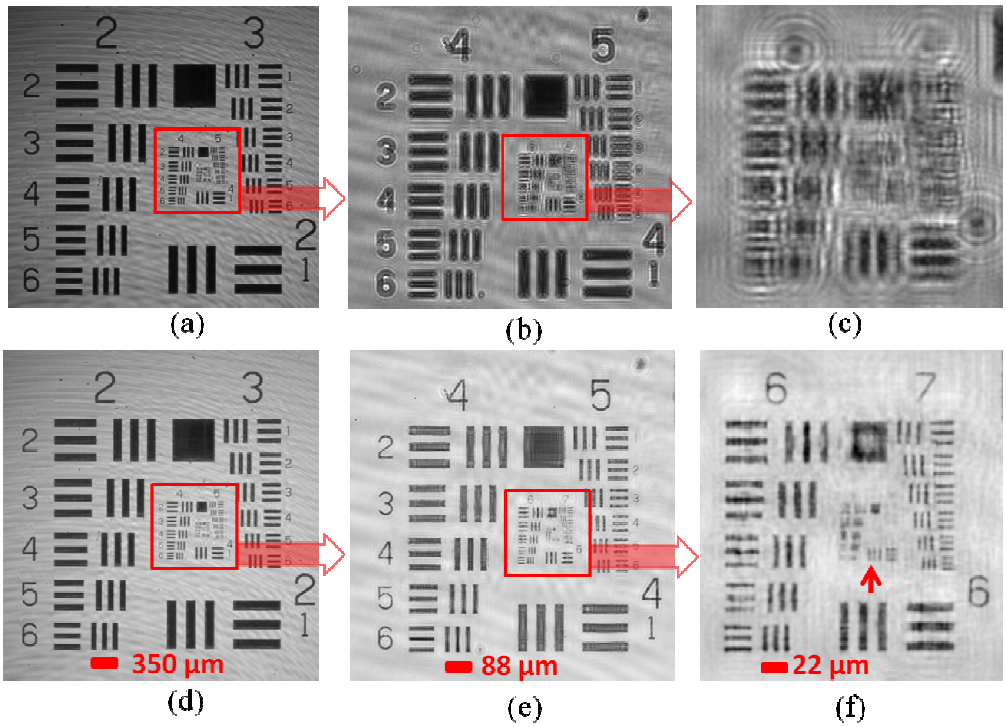

Fig. 5. Demonstration of the imaging performance of our in-line lensfree transmission microscope shown in Fig. 2. (a-c) Raw lensfree in-line transmission holograms for (a) groups 2-3, (b) groups 4-5, and (c) groups 6-7 of the US-AFT. The corresponding reconstruction results (amplitude) are shown in (d), (e), and (f), respectively.

3. Experimental results and discussion

Figure 3 illustrates the reconstruction procedures of our lensfree off-axis reflection holographic microscope shown in Fig. 1. To quantify the performance of its resolution and FOV, we first imaged a US Air Force resolution test target (US-AFT), i.e., USAF 1951 Test Chart from Edmund Optics. The raw lensfree hologram of the US-AFT is recorded using the reflection set-up of Fig. 1 as shown in Fig. 3(a). Note that the interference fringes between the reference and the reflected object waves are clearly visible within the expanded frame of Fig. 3(a). This lensfree reflection hologram is then digitally interpolated and padded with zeros (see Fig. 3(b)) and its corresponding 2D Fourier spectrum is also shown in Fig. 3(c). Note that as a result of the off-axis recording geometry, the spatial frequencies of the real and twin images are clearly separated from the 0th order [2]. Furthermore, some of the parasitic reflections [6] occurring at various interfaces in our experimental setup also appear in Fig. 3(c), marked with yellow dashed arrows. After spatial filtering of these unwanted frequency components, our lensfree reflection hologram can be rapidly reconstructed using the Fresnel approximation [6,31] to yield the image of the AFT over a rather large FOV of ~9 mm^2, as shown in Fig. 3(d). Figure 3(e) also shows a digitally enlarged version of the central section (taken from Fig. 3(d) indicated by the yellow dashed rectangular box), which demonstrates ≤2 µm lateral resolution.

Next, using the same off-axis lensfree reflection microscopy mode (i.e., Fig. 1c), we imaged a histopathology slide (prepared using standard sample preparation protocols [46]) corresponding to a human skin tissue, the results of which are summarized in Fig. 4. To minimize multiple reflection interference artifacts in our reflection hologram, we used a right angle prism behind the glass sample holding the tissue slide with refractive index matching oil between the two. Since the intensity of the reflected wave from the skin tissue is quite weak, a

#150686 - $15.00 USD Received 7 Jul 2011; revised 11 Aug 2011; accepted 11 Aug 2011; published 30 Aug 2011

regular thin cover glass (thickness ~100 μm) is used as a reference mirror in Fig. 1 to balance the intensity between the object and the reference waves. Figure 4(a) shows the lensfree off-axis reflection hologram of this skin tissue, where a digitally expanded version of it is also shown in Fig. 4(b). The reconstruction result of this off-axis reflection hologram is shown in Fig. 4(c). For comparison purposes, Fig. 4(d) also illustrates the results of a conventional reflection mode bench-top microscope imaging the same specimen taken with a 4X objective lens (0.1 NA), which agrees well with our field-portable lensfree reflection microscope results. Note that due to their limited FOV, higher magnification objective lenses (e.g., 10X or 20X) would not be able to capture the same comparison image.

Following this, we tested the imaging performance of our transmission mode field-portable microscope shown in Fig. 2. To demonstrate its resolving power, lensfree in-line hologram of an AFT is recorded using the set-up shown in Fig. 2, where the raw holograms of groups 2 & 3, groups 4 & 5, and groups 6 & 7 are shown in Figs. 5(a), 5(b), and 5(c), respectively. The corresponding reconstructed amplitude images of these lensfree transmission holograms are shown in Figs. 5(d), 5(e), and 5(f), respectively. These images are digitally obtained by an iterative reconstruction process (~15 iterations) that is based on object-support constrained phase recovery, which effectively removes the twin image artifact of in-line holography [3,18,32]. The reconstructed images shown in Fig. 5 demonstrate a resolution of ≤2μm over a wide imaging FOV of ~24 mm^2 which is due to our unit-fringe-magnification hologram-recording geometry. It is important to note that our off-axis lensfree reflection microscope provides a similar spatial resolution, however, over a smaller FOV of ~9 mm^2. This relatively reduced FOV of the reflection mode is due to its increased fringe magnification (F ~1.67 compared to F ~1 in transmission mode) as well as due to its off-axis geometry with θ ~5°.

And finally, we imaged 4-μm-sized micro-particles using the same lensless holographic transmission microscope. Figure 6 illustrates our lensfree holographic imaging results and also provides comparison images of the same objects obtained by a 40X objective lens (NA = 0.6) of a conventional bench-top bright-field microscope, which provide a decent agreement to our reconstruction results.

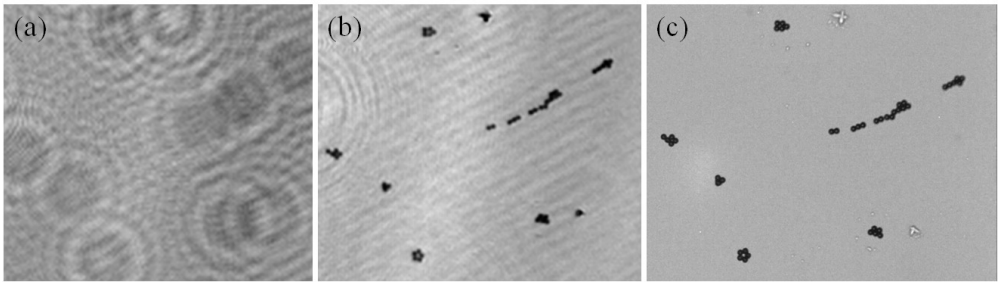

Fig. 6. (a) Raw lensfree transmission hologram for 4 μm beads and (b) its corresponding reconstructed amplitude image are illustrated. (c) Conventional bright-field microscope image of the same objects (40X objective lens – NA: 0.6) is also provided for comparison purposes.

We should note that this presented field-portable microscope could be used to monitor e.g., water samples as well as various bodily fluids such as semen or blood. In its transmission geometry, a major advantage of this platform is its imaging volume. The large FOV (~24 mm^2) combined with a long depth-of-field (e.g., ~1-2 mm) can enable rapid screening of large sample volumes. For water quality monitoring applications, for instance, the reflection mode would also be quite relevant, especially for sample concentration steps that involve e.g., porous silicon membranes, where the reflection mode geometry could be of great interest with its large imaging FOV (e.g., ~9 mm^2)

#150686 - $15.00 USD Received 7 Jul 2011; revised 11 Aug 2011; accepted 11 Aug 2011; published 30 Aug 2011

4. Conclusion

We demonstrated a field-portable lensless microscope that can image specimens in both reflection and transmission modes using off-axis and in-line digital holography, respectively. We tested the performance of this compact dual-mode microscope by imaging a US-air force resolution test target, various micro-particles as well as a histopathology slide. Due to its compact, cost-effective, and lightweight design, this dual-mode lensless holographic microscope could be useful in field conditions and in resource-limited locations.

Acknowledgments

A. Ozcan gratefully acknowledges the support of NSF CAREER Award, the ONR Young Investigator Award 2009 and the NIH Director's New Innovator Award DP2OD006427 from the Office of The Director, NIH. The authors also acknowledge the support of the Gates Foundation, Vodafone Americas Foundation, and NSF BISH program (under Awards 0754880 and 0930501). The authors also acknowledge Derek Tseng of UCLA for his assistance with the figures.

#150686 - $15.00 USD Received 7 Jul 2011; revised 11 Aug 2011; accepted 11 Aug 2011; published 30 Aug 2011